CHARACTERIZING THE MECHANICAL AND STRUCTURAL PERFORMANCE OF HYDRAULIC-LIME CMU WALL COMPONENTS AND ASSEMBLIES

by

Tucker Trostel Haunt

A thesis submitted in partial fulfillment
of the requirements for the degree

of

Master of Science

In

Civil Engineering

MONTANA STATE UNIVERSITY
Bozeman, Montana

May 2015

ACKNOWLEDGEMENTS

I would like to express my gratitude to my advisor, Dr. Mike Berry, who guided me through my research and coursework at Montana State University. I would also like to recognize the other members of my committee, Dr. Jerry Stephens, Dr. Damon Fick and Mr. Anders Larsson for their contributions to my research and education.

An additional note of gratitude goes out to all those associated with Namchak and Virginia Lime Works. Specifically, Geoff Bandenoch and Jimmy Price, who made this research possible. I would also like to thank the engineers from BCE Structural, Tom Beaudette and Sam Fox, for their support and advice. Finally, I would like to thank John Neuhaus, from Kanta Products, who worked with the design team to produce the lime CMU blocks, and shared his knowledge of CMU with the research team.

Finally I would like to acknowledge and thank my fellow students who helped me with my lab testing along the way. Specifically, I would like to thank Brian Zirbel, Rick Snidarich, Jackson Kunz, Calvin Reahard, and Ammon Grosebeck for their help in the preparation and testing of the many specimens used throughout this research. I also would like to thank Dave Walters and Ladean McKittrick for their assistance with the 3D strain-field camera.

TABLE OF CONTENTS

TABLE OF CONTENTS - CONTINUED

LIST OF TABLES

LIST OF FIGURES

Figure Page

LIST OF FIGURES - CONTINUED

Figure Page

LIST OF FIGURES - CONTINUED

Figure Page

ABSTRACT

Concrete is the most commonly used building material in the world. As a result, the production of portland cement accounts for seven percent of the carbon dioxide produced by industry worldwide. A more environmentally-friendly alternative to portland cement could significantly reduce carbon dioxide emissions, and thus reduce the carbon footprint of the concrete industry. One possible alternative to portland cement is hydraulic lime, which creates less carbon dioxide during its production than portland cement. Further, hydraulic lime reabsorbs carbon dioxide as it cures, through carbonation. Despite these advantages, there are some logistical issues associated with using hydraulic lime in modern construction (e.g., increased cure times). Using hydraulic lime in concrete masonry units provides an opportunity to overcome some of these limitations and thus take advantage of the environmental benefits associated with its use. While the use of lime as the binder in masonry construction is not a new concept, modern building codes have evolved around components made with portland cement rather than hydraulic lime.

The, research discussed herein investigates the mechanical and structural performance of hydraulic lime masonry components, and evaluates the efficacy of simple mechanics models used to predict their performance. First, the performance of individual masonry components (i.e., mortar, grout, and block) are evaluated, followed by an evaluation of simple masonry assemblies (e.g., prisms). Finally, a series of five wall assemblies were tested to determine the in-plane shear resistance of hydraulic-lime wall systems. It was found that while the strength of the hydraulic lime masonry components/assemblies were significantly less than those made with portland cement, the use of hydraulic lime in this application is feasible.

INTRODUCTION

Background

Masonry has been one of the most widely used building materials in the world for the last several thousand years due to the fact that it is versatile, relatively inexpensive, and durable. In modern construction, concrete masonry units (CMU), using portland cement as binder, have largely replaced stone and brick masonry in structural applications; this is due, in part, to their ability to incorporate reinforcing steel. Standard CMUs use portland cement as the primary binder; however, the production of portland cement has significant environmental impacts, and therefore an investigation into the use of less environmentally taxing materials is warranted.

In 2013 the United States alone produced 77.2 million tons of portland cement for use in concrete and masonry construction (Oss, 2014). Worldwide, the production of portland cement has been reported to generate seven percent of the annual carbon dioxide emissions produced by industry (Preuss, 2013). In an effort to reduce industrial environmental impacts, starting in 2015 cement plants in the United States will be required to comply with the 2010 National Emissions Standards for Hazardous Air Pollutants, a standard that many cement plants are poorly equipped to meet (Oss, 2014). Investigating less energy intensive concrete binders may aid in reducing the carbon footprint of the concrete industry.

Portland cement is created by burning a mixture of limestone and clays at 1450 degrees Celsius, producing 1638 lb of CO_2 per ton of binder (Revie, 2013). By contrast, hydraulic lime is created at temperatures between 900 and 1100 degrees Celsius and

produces only 1320 lb of CO_2 per ton of binder. Unlike portland cement, which does not reabsorb any significant amount of carbon dioxide, as a hydraulic lime concrete cures it will reabsorb about 48% of the CO_2 produced in creation of the lime binder via carbonization (Revie, 2013). The reduced energy consumption and emissions associated with the production of lime binders relative to portland cement is just one of the beneficial properties of hydraulic lime as a binder in concrete, as hydraulic lime cements have been known to be extremely durable.

The first use of lime as a binder dates back to early Greek and Roman masonry construction. The Greeks and Romans burned pure limestone to form quicklime (CaO) to use in mortars. After CaO is mixed with water, strength is gained through carbonization (Revie, 2013), the chemical reaction that returns the lime to its original chemical compostions $CaCO_3$ (Hartshorn, 2012). This chemical reaction requires dry conditions; therefore, the use of quicklime in harsh or wet environments is impractical. However, the ancient Romans discovered that by either burning dolomitic limestone (a limestone containing impurities) or by adding pozzolans (in the form of volcanic sands) to quicklime, they could produce a binder that was significantly more durable and could set in the presence of water. This variation to the traditional quicklime binder created the hydraulic limes used in many ancient Roman structures, some of which are still around today.

Some of the first uses of hydraulic-lime concretes were in harsh conditions such as harbors and breakwaters. The concretes in this application have performed exceptionally well in these challenging conditions for over 2000 years. Preuss (2013)

investigated ancient Roman seawater concretes to determine the reasons for their exceptional durability, and found that their increased durability relative to portland cement concrete is most likely due to the inclusion of aluminum-rich pozzolans and the subsequent effects these have on the hydration products. Portland cement forms chemical bonds called calcium-silicate-hydrates (C-S-H), whereas ancient Roman lime concretes were found to have more stable bonds formed from a calcium-aluminum-silicate-hydrate (C-A-S-H). Furthermore, Preuss (2013) found that the ancient seawater concretes contained aluminum tobermorite, a naturally occurring ideal crystalline structure that is thought to contribute to these concretes' exceptional durability. The service life of modern buildings and bridges could be greatly increased if this durability could be harnessed in modern construction, leading to a long-term reduction in the demand for concrete and the negative environmental impacts associated with its production.

The lime binder used in this research is a dolomitic lime that is mixed with a pozzolan to increase the hydraulic nature of the lime. A typical dolomitic lime gains strength through the carbonization of calcium hydroxide ($Ca(OH)_2$) and magnesium hydroxide ($Mg(OH)_2$). The calcium hydroxide carbonates to calcium carbonate (the same end product as the quicklime cycle), and the magnesium hydroxide carbonates to magnesium carbonate. The reactions creating calcium carbonate occur quickly, accounting for much of the early strength gain in dolomitic lime concretes. Magnesium carbonate carbonates at a much slower rate, adding to the long-term strength gain of dolomitic limes (Schork, 2012). These carbonization reactions lead to the reabsorption of

CO_2, which is in large part responsible for the environmentally desirable nature of hydraulic limes. In addition to carbonization, the lime in this research gains strength from hydration reactions occurring between the dolomitic lime and the added pozzolan. While the exact pozzolan used in this research is proprietary and unknown to the researchers, the effect of including pozzolans is similar for many conventional pozzolans. Conventional pozzolans generally consist of silica and alumina that react with calcium hydroxide in the presence of water to create the hydration bonds (Mertens, Snellings, Van Balen, Bicer-Simsir, Verlooy, & Elsen, 2008).

Despite the benefits of using hydraulic lime in lieu of portland cement, there are some disadvantages that hinder its use in modern construction. For example, hydraulic limes take longer to gain strength relative to portland cement. When referring to compressive strengths, hydraulic lime concrete strengths are typically cited at 120 days, while conventional portland cement strengths are cited at 28-days. Further, and possibly more importantly, there is the challenge of educating those responsible for batching and placing the concrete, as these processes would be altered relative to conventional concrete. This drawback has been noted as a hindrance in the adoption of other newly developed concrete methodologies (Berry, Stephens, & Cross, 2011; Cross, Stephens, & Berry, 2010; Berry, Kappes, & Schroeder, 2014).

These limitations of hydraulic lime concretes could be overcome by using them in concrete masonry units rather than in cast-in-place applications. In this application, the blocks could be cured (for the longer time period) at the masonry block plant prior to their arrival at the construction site, thus not delaying the on-site construction time.

Further, only the workers at the masonry block plant would need to be educated/trained in the intricacies of working with this material. In addition to the advantages in education, block plants serve a larger geographic area compared to a typical concrete batch plant, leading to better distribution of the new technology. Therefore, using hydraulic lime in concrete masonry units would allow for the environmental benefits of doing so, without the limitations associated with delayed strength gain and training.

It should be noted that the use of hydraulic lime in masonry is not new, as hydraulic lime was one of the primary binding components in masonry construction prior to the introduction of and migration to portland cement in the early 1800s. However, modern research has focused on the use of portland cement based components, and therefore current material specifications and building codes have evolved around the use of portland cement rather than hydraulic lime. Therefore, research is required to characterize the performance of concrete masonry components made with hydraulic lime, as well as to ensure applicability of the design methodologies prescribed within the building codes.

The research presented in this thesis stemmed from an owner's desire to use an innovative material to construct a large environmentally-friendly and durable building in western Montana. Specifically, the owner was interested in using hydraulic-lime CMU walls as cladding for their building, and as the primary lateral-force resisting system within the structure. The Civil Engineering Department at Montana State University (MSU) was hired to investigate the mechanical and structural performance of the hydraulic-lime concrete masonry units and assemblies to be used in the construction of

this building, and to investigate the applicability of simple mechanics models that may be used to predict their performance. Further, the thermal resistivity of the wall system was also studied by MSU; however, this thermal testing is beyond the scope of this thesis.

Research Objective

The primary objective of this thesis is to characterize the performance of CMU wall systems made with hydraulic lime as the sole binder. This study includes a characterization of the mechanical properties of each of the individual elements within the wall system (i.e. mortar, grout and CMU), as well as the masonry wall as a whole. This research is a necessary step in using hydraulic lime CMUs in modern construction.

Research Scope

The research objectives were accomplished through the completion of the following tasks:

1. The materials used in the individual masonry components were evaluated.
2. The mechanical properties of the individual masonry components were characterized.
3. Five masonry walls were constructed and tested under in-plane lateral loads.

These tasks are discussed in depth in the following chapters. Chapter 2 presents the chemical composition of the lime binders, and provides a description of the mortar, grout, and lime CMU. The compression strengths of mortar, grout, and blocks are presented in Chapter 3. In Chapter 4 the results of mechanical testing on masonry assemblies are presented. A detailed description of the wall tests are discussed in Chapter

5, along with a discussion of the results of these tests. Finally, this research is summarized and conclusions are drawn in Chapter 6.

MATERIALS

The materials used in this research are discussed in this chapter. These materials include the hydraulic lime binder, the mortar, the grout, and the hydraulic-lime concrete masonry units.

Lime

The hydraulic lime used throughout this research is a product designed, produced, and provided by Virginia Lime Works from Madison Heights, Virginia. As was recommended by the manufacturer their Building Lime 150 was used for the mortar and grouts (due to its flexibility), while their Building Lime 500 was used in the masonry units (due to its increased stiffness and strength). While the exact makeup of these binders is proprietary, and unknown to the researchers, it is believed that both binders use the same dolomitic lime as a base, with the primary difference between them being the amount of added pozzolan. This pozzolonic admixture is included to induce hydration in the binder, and increase the short-term strength gain.

The effect that the dolomitic-lime base has on the performance of the Building Lime products discussed above was also investigated in this research. In particular, two hydraulic-lime sources were studied. One lime was from a Graymont plant in Eden, Wisconsin and the other was from a Graymont plant in Genoa, Ohio (Graymont Western lime Inc., 2013; Graymont Dollme Inc., 2012). The Ohio sourced lime has been used previously in Virginia Lime Works projects, while the Wisconsin lime was used for the

first time in this research. The chemical and physical composition of these limes are provided in Table 1.

Table 1. Chemical composition of the Wisconsin and Ohio Dolomitic Limes

Source	Quciklime Components		Hydrated Lime Components								Physical Properties	
	CaO (%)	MgO (%)	Loss on Ignition (%)	$Ca(OH)_2$ (%)	$Mg(OH)_2$ (%)	SiO_2 (%)	Fe_2O_3 (%)	S (%)	H_2O (%)	$CaCO_3$ (%)	Desity (lbs/ft^3)	Surface (cm^3/g)
Wisconsin	41.5	29.5	26.1	50.5	34.3	1.9	0.3	0.6	0.8	5.7	25-37	36000
Ohio	41.7	30.2	26.9	55.1	43.7	0.3	0.2	0.1	0.5	8.5	28-43	28160

Referring to this table, there are subtle differences between these two limes, with the Ohio lime having higher percentages of many of the chemicals important in the processes of carbonation and hydration, which were discussed previously. Most notably the $Ca(OH)_2$ (the chemical precursor of short-term carbonation) and $Mg(OH)_2$ (the chemical precursor of the long-term carbonation) have significantly higher concentrations in the Ohio lime than the Wisconsin lime. Further, there are some important differences between the two limes relative to possible hydration reactions. However, it is difficult to determine the extent that these differences will have on the performance of the limes because the amount and type of added pozzolan are unknown to the researchers. That being said, most pozzolanic reactions are between silica and alumina, and calcium hydroxide (Mertens, Snellings, Van Balen, Bicer-Simsir, Verlooy, & Elsen, 2008), which is almost 5% higher in the Ohio lime than the Wisconsin lime. Further, magnesium is also known to be active in hydration reactions; therefore, higher concentrations of magnesium in the Ohio lime may lead to better early strength gain relative to the Wisconsin lime.

Aggregates

Three types of aggregate were used in the masonry components in this research: masonry sand, concrete sand, and coarse aggregate. The masonry sand was in substantial accordance with the gradations prescribed in ASTM C144 (ASTM International , 2013), and was used in both the mortar and the grout. The concrete sand used in the grout was in substantial accordance to the fine aggregate requirements in ASTM C33 (ASTM International, 2013). Finally, a 3/8-inch-minus course aggregate was used in the grout, and was in substantial accordance with the grading requirements for the Course Aggregate Size No. 89 prescribed in ASTM C404 (ASTM International, 2013).

Mortar

Mortar was prepared for two different scenarios in this research; in particular, it was prepared for mortar specific tests and it was prepared for use in the masonry assemblies. The preparation method varied between these scenarios. In the mortar specific tests, the mortar was prepared by first mixing 1 part lime to 2.5 parts masonry sand, and then adding enough water to obtain a flow of 110+/-5%, which is specified by ASTM C1712 (ASTM International, 2013). For the masonry assemblies and wall specimens, this procedure was somewhat less controlled. Mortar in these specimens was mixed with 1 part lime to 2.5 parts sand, and water was added to obtain the desired consistency for construction. The mortar binder in both cases was Virginia Lime Works Building Lime 150, with the Wisconsin dolomitic lime as the base.

Grout

Two different grout mixes were investigated in this research: a structural grade grout consisting of conventional aggregates and hydraulic-lime binder, and a grout consisting of a perlite fill and the hydraulic-lime binder. The structural grout was intended to increase the structural capacity of the assemblies and walls, while the perlite grout was included as an insulator, and was not anticipated to contribute structurally to the system. The binder in both cases was Virginia Lime Works Building Lime 150, with the Wisconsin dolomitic lime as the base.

Structural Grout

The structural grout consisted of 3 parts aggregates to 1 part Building Lime 150. In particular, the aggregate included 5 parts of the masonry sand, 3 parts of the concrete sand, and 2 parts of the 3/8" minus course aggregate. This combination of aggregates was determined to have a good distribution of aggregate sizes, and resulted in a very workable grout. The grout was prepared by first adding aggregates and lime, and then including enough water to achieve a mix that could be easily poured into the wall specimens without separation. Structural grout compression specimens were prepared using the methods described in ASTM C1019 (ASTM International, 2013).

Perlite Grout

The perlite grout consisted of two bags of perlite (25 ft^3 per bag), provided by Virginia Lime Works, to one bag of Building Lime 150 (50 lbs). As with the structural grout, these components were mixed in a small concrete mixer and water was then added

until the mixture was pourable. By observation, this grout would have very little compressive strength due to the large quantity of perlite; thus, no compression specimens were prepared from this grout.

Lime Concrete Masonry Unit

The lime concrete masonry units used in this project were produced by the Kanta Products CMU plant in Three Forks, Montana. Two block types were investigated in this research: a standard proprietary lightweight block, and a modified normal-weight block. It should be noted that the standard blocks were manufactured prior to the research team becoming involved in this project, and were used in the construction of the assembly specimens (e.g., prisms and tensile assemblies), as well as in the wall specimens. Once preliminary strength tests were performed on the standard block, the modified block was pursued in an attempt to improve the strength. These modified blocks were also used to investigate the effects of the different lime sources discussed in a previous section. While both of these mix designs are proprietary and cannot be disclosed herein, they both included a mixture of local shale, and local fine and coarse aggregates.

Block Production

All blocks were cast using Kanta Product's Besser V312 block machine. The V312 block machine casts blocks three at a time and is capable of producing 1200 blocks per hour. The aggregates, binder, and water are batched and mixed by an automated system, and then fed into the block machine. The concrete mix goes from the mixer to the feed drawer, where it is shaken into a mold. Next a vibrating head compacts the concrete

until it reaches a standard height, at which time they exit the machine (Figure 1). Before the blocks are palletized, they are given time to gain strength, either through steam curing in a kiln or left to air dry.

Figure 1. Freshly cast lime CMU block

It should be noted that the curing method of the standard lightweight blocks is unknown to the researchers, as these blocks were manufactured prior to their involvement. The modified blocks, however, were cured based on recommendations from Virginia Lime Works. Specifically, the blocks were first air dried for four hours, and then steam cured for five. The blocks were then palletized and stored inside at Kanta for two weeks, prior to being transported to MSU, where different curing methods from this point on were investigated.

Dimensions

Both types of lime blocks used in this research met the dimensional requirements for lightweight eight-inch nominal block prescribed by ASTM C90 (ASTM International, 2013) (Figure 2). These blocks are nominally 8 inches wide and tall, and 16 inches long.

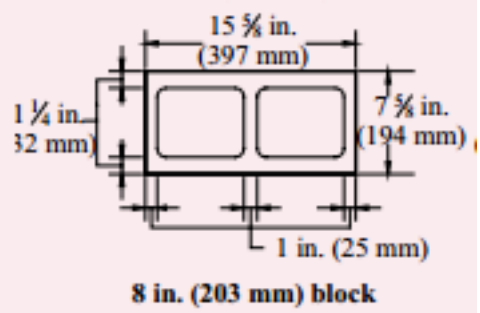

Figure 2. Standard block dimensions (National Concrete Masonry Association, 2007)

COMPRESSIVE STRENGTH OF MASONRY COMPONENTS

In this chapter, the compressive strengths of the individual elements of the masonry components are examined. Compressive strength is investigated, as it is arguably the most important property of concrete masonry components. That is, CMU components are loaded primarily in compression, and compressive strength often has well documented relationships with other material characteristics (e.g., shear resistance, stiffness, durability).

First, the compressive strength of the mortar under varying curing conditions is studied, followed by the compressive strength of the structural grout. Finally, the compressive strengths of the lime CMU blocks is investigated, which includes characterizing the effects of different lime binders and varying curing conditions.

Mortar

Two curing methods (i.e., dry and moist), and their subsequent effect on compressive strength were investigated in this research. These two curing methods were intended to bracket the curing conditions that would be seen onsite during construction. At 24 hours, the dry-cure specimens were removed from their molds and placed in the lab, while the moist cure specimens were placed in a 100%-humidity cure room until the day of testing.

A total of 20 2-inch cube specimens were tested for each curing method: two samples per week for ten weeks. The specimens were tested in compression until failure in substantial accordance with ASTM C109 (ASTM International, 2013). The observed

strengths of theses mortar specimens over time are shown in Figure 3. As can be observed in this figure, both mortars continued to gain strength over time, with the gains becoming less pronounced with time. The dry-cured specimens gained strength quicker, and hit a higher compressive strength on every test day, with the dry-cure specimens obtaining a final compressive strength of 510 psi. The moist-cure specimens achieved a strength of only 400 psi. The increased strength of the dry-cure specimens relative to the moist-cured specimens may be associated with reduced carbonation in the moist-cured samples, as carbonation cannot occur as effectively above 75% humidity.

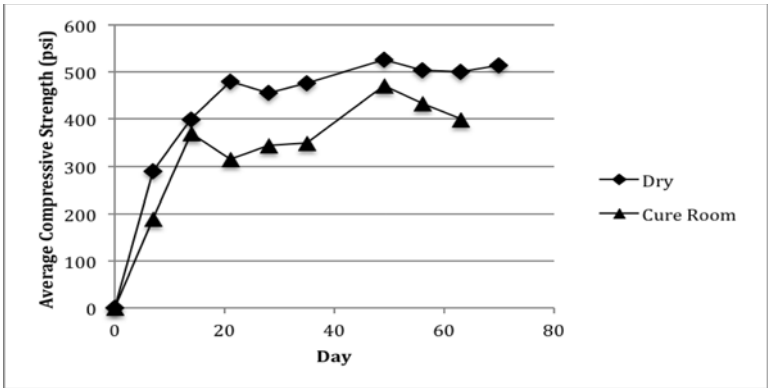

Figure 3. Mortar compressive strengths for varying curing regimens over time

For comparison, portland cement based specimens were prepared and tested following the same procedure employed for the lime masonry samples. They were cured in the same method as the moist-cured hydraulic lime mortar. The compressive strength of these portland control specimens was 1220 psi and 1925 psi at 28 and 56 days, respectively. This is nearly four times what was observed for the hydraulic lime samples.

Because the dry-cured mortar samples yielded the strongest and most consistent results, it was decided to dry cure all masonry assemblies in this research (e.g., prisms and walls).

Grout

The compressive strength of the structural grout used in the masonry components and walls was tested in this research. These grout specimens were collected and cured in substantial accordance with ASTM C1019 (ASTM International, 2013). The grout was cured alongside the wall specimens that will be discussed in a later section, and was tested at approximately same time as the walls. This was done in order to provide an estimate of the grout strength within the walls. The average compressive strength of the grout at 420 days was determined to be 320 psi.

The decision was made to not test the structural capacity of the perlite grout. The primary purpose of the perlite grout is to provide insulation, and it is known to have a very low compressive strength. In addition, as the masonry assemblies cured the perlite grout was observed to shrink away from the cell walls. The shrinkage did not allow for load transfer to the perlite; therefore, the perlite was not considered to have any effect on the overall structural performance of the masonry system.

Lime Masonry Blocks

As discussed in the Materials Chapter, two separate block types were investigated in this research: a standard lightweight block and a modified normal-weight block. The standard blocks were manufactured prior to the research team becoming involved, and

the modified block was perused to in an attempt improve the strength of the blocks. Further, the modified blocks provided an opportunity to investigate the effect of the lime binder source and varying curing methods.

The capping methods used in this research are discussed below, followed by the results of compression tests on the standard and modified blocks.

Capping Methods

Several capping methods were investigated in this research. The caps are included to distribute the compressive forces evenly across the CMU block. ASTM C1552 (ASTM International, 2013) allows CMU blocks to be capped using either a sulfur compound or gypsum cement. Both of these capping methods are very time consuming and expensive; therefore, a cheaper and less labor intensive capping method was investigated to determine if it would be suitable for this project. In particular, fiberboard was investigated to determine if it could be used without adversely affecting the accuracy of the results. Previous research has indicated that fiberboard caps can give comparable results to ASTM standard capping practices (Ballard, 2012).

For this investigation, a total of twelve blocks were capped and tested. Six of these blocks were capped using fiberboard and six were capped in accordance to ASTM C1552 using a sulfur compound. Based on this study, it was found that the blocks capped with the sulfur compound had an average compressive strength of 1090 psi with a coefficient of variation of 11.4%. The blocks capped with fiberboard had an average compressive strength of 1020 psi and a coefficient of variation of 3.5%. These results indicate that the fiberboard capping method would be suitable for this research, as the

fiberboard specimens had a similar average compressive strength as the sulfur-capped specimens, with a smaller coefficient of variation. Therefore, fiberboard capping was used throughout the duration of this project due to its ease of use.

Standard Blocks

The standard blocks were tested in substantial accordance to ASTM C140 (ASTM International, 2013) over the course of 130 days, and the results of this testing are shown Figure 4.

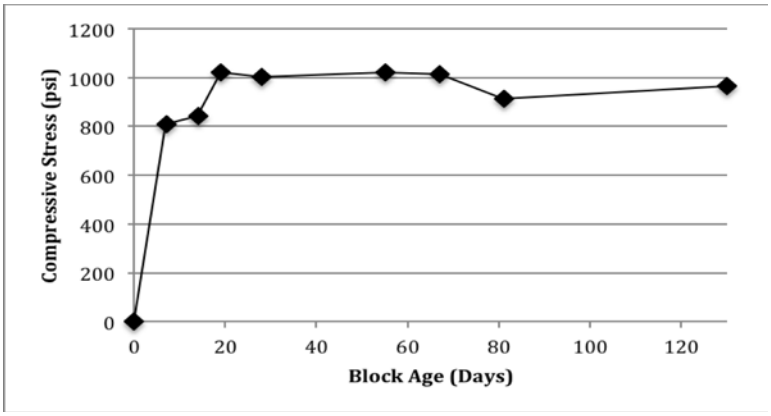

Figure 4. Compressive strength of standard block vs time

This block design saw significant strength gains over the first three weeks, at which time the strengths plateaued at approximately 1000 psi. This is about half the strength that is required in the ASTM C90 for standard CMU. As stated previously, a modified block was pursued in an attempt to increase this strength.

Modified Blocks

In this study, a normal-weight block design was employed in an attempt to achieve higher strengths. This study also provided an opportunity to investigate the effect of different lime sources and curing methods. In this investigation, two separate runs of this modified design were produced; one using the original Wisconsin based lime binder, the other using the binder from Ohio. It was hoped that due to its favorable chemical makeup, the blocks using the Ohio lime would produce higher capacity blocks. After casting, these blocks were divided into three different groups and subjected to differing curing regimens. Three blocks from each lime source and each curing method were tested in compression each week over the course of 7 weeks (a total of 18 blocks each test day). All blocks were tested in substantial accordance with ASTM C140.

Standard Block vs Modified Block The effect of block design can be isolated by comparing the modified dry-cured Wisconsin block strengths to the standard block strengths from the previous section (which also used Wisonsin lime and were dry cured), as is done in Figure 5.

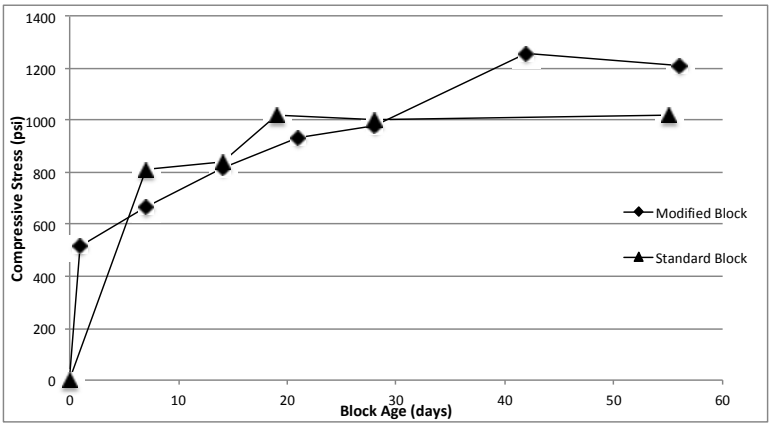

Figure 5. Standard block and modified block vs time

Referring to this figure, the modified block strength is less than the standard block initially; however, its strength surpasses the standard block at 28 days and remains higher throughout the testing period. At 56 days the modified block had a strength of approximately 200 psi higher than the standard block. There were a limited number of modified blocks for this study, therefore modified blocks could not be tested after the 56 days shown above. However, the standard blocks were tested as far out as 130 days (Figure 4), and these strengths were still hovering around 1000 psi. These results indicate that the modified normal-weight block design may be more appropriate for future projects, as it resulted in higher strengths.

Wisconsin Lime vs Ohio Lime The effect of lime source can be isolated by comparing the Wisconsin-based lime blocks to the Ohio-based lime blocks, as is done in Figure 6. In this figure, for clarity, only the dry-cure specimen results are shown; however, a similar trend was observed for the moist-cure specimens.

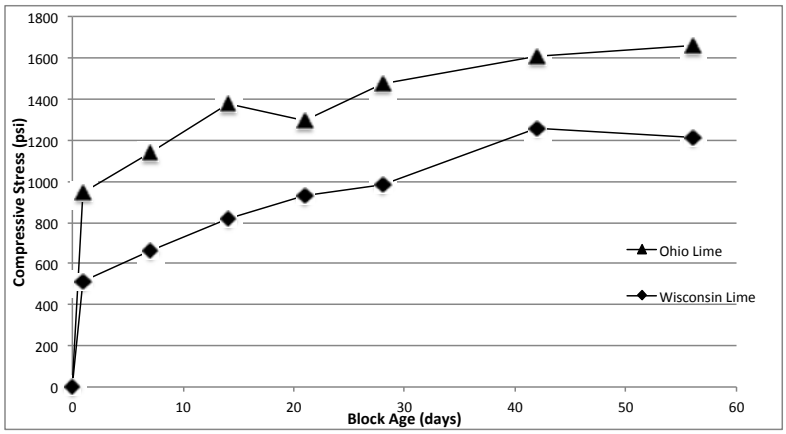

Figure 6. Compressive strength of Wisconsin lime vs Ohio lime

In regards to the effect of lime source on the strength of the modified blocks, the Ohio lime blocks were significantly stronger than the Wisconsin lime blocks on every test day. This result was somewhat expected based on differences in the chemical composition of the two lime sources, as discussed in the Materials chapter. In particular, the Ohio lime contains a larger fraction of magnesium hydroxide and calcium hydroxide, which have been known to contribute to the hydration reactions and subsequently may result in earlier strength gain. To investigate this further, the ratio of Ohio strength to Wisconsin strength is shown in Figure 7. As can be observed in this figure, the Ohio lime is approximately 80 percent stronger the day after testing, but then this strength difference decreases to around 37 percent at 56 days. Indicating that differences may be most significant for early strength gain. The early strength gain observed in the Ohio lime would be favorable for manufacturing/transportation/construction, as the blocks would not need to cure for as long. It should also be noted that while the Ohio blocks did not

reach the minimum specified block strength by ASTM C90, they were fairly close at 1665 psi.

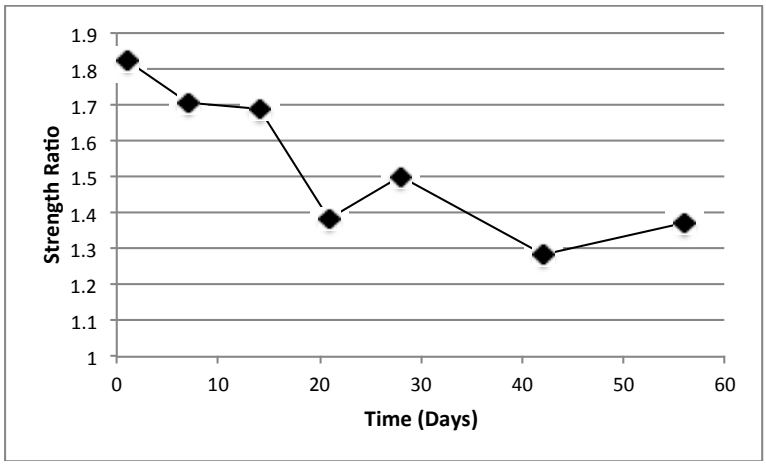

Figure 7. Ratio of Ohio to Wisconsin compressive strength vs time

Curing Methods Three different curing methods were considered in the modified block testing. After 14 days at the Kanta Products facility, the modified blocks were moved to the MSU labs and subjected to different curing regimens. To bracket the possible conditions that may be experienced in the field, a third of the blocks were dry cured and a third of the blocks moist cured in a standard concrete cure room at 100% humidity. The final third were stored in a cold room at -40 degrees Celsius for two weeks and then brought back to room temperature for four weeks. This was done to examine the effects of freezing temperatures on the hydration and carbonization processes. The average compressive strengths for the Ohio and Wisconsin lime blocks over time are provided in Figure 8 and Figure 9, respectively.

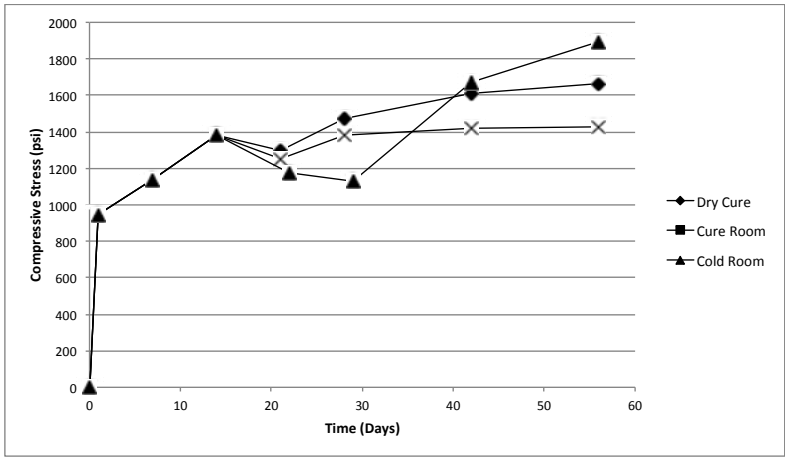

Figure 8. Compressive strength of modified block using Ohio lime for various curing methods

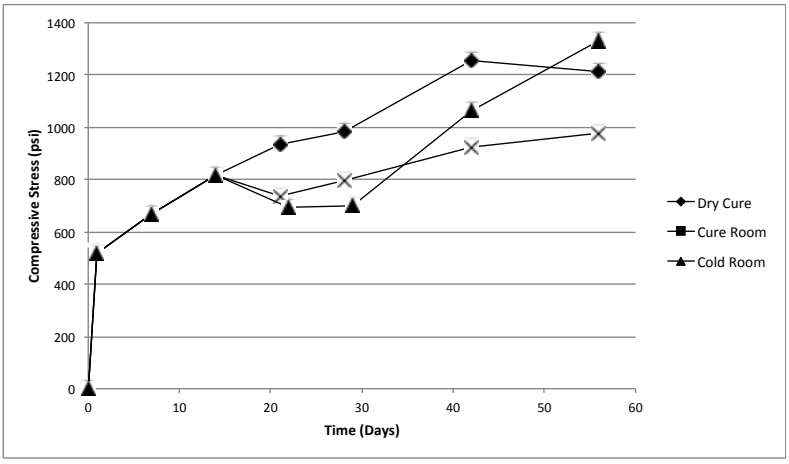

Figure 9. Compressive strength of modified block using Wisconsin lime for various curing methods

As can be observed in these figures, for both lime binders, curing specimens under dry conditions results in higher strengths than moist curing. This is consistent with what was observed for mortar specimens in an earlier section. Relative to the effect of freezing, it can also be observed that although freezing has an immediate negative impact

on strength, this impact is temporary. Once the specimens were removed from the freezer at 28 days, their strength increased to and even surpassed the strengths of the specimens that were simply dry cured from the beginning. This trend is similar to what is observed in conventional concrete.

MECHANICAL PROPERTIES OF MASONRY ASSEMBLIES

In this chapter the composite mechanical properties of masonry assemblies are presented. While some design properties may be inferred from the mechanical properties of individual masonry elements, it is important to also consider how the masonry system will behave compositely. In particular, this section presents results on the compressive behavior of two-block prisms, and the tensile behavior of multiple block assemblies. It is important to note that the specimens in this chapter were made with the standard blocks discussed in the previous section.

Compression Prisms

The compressive response (strength and modulus) of two types of fully-grouted two-block prisms were tested in this research. The first type of prism was grouted with the structural grout discussed in a previous section, while the second was grouted with the perlite grout. These prisms were constructed by experienced masons at the same time as the wall specimens discussed in the following chapter. A picture of the construction process is shown in Figure 10. They were also cured alongside the wall specimens at room temperature without added moisture.

Figure 10. Construction of prisms

It should also be noted that both the structural and perlite grout had a tendency to shrink when placed in the CMU blocks, although it was significantly less in the structural grout. A perlite-grouted specimen is shown in Figure 11.

Figure 11. Shrinkage of perlite grout in prism

The perlite grouted prisms were capped using fiberboard, as was used in the block tests, while the structurally grouted prisms were capped using a sulfur-capping compound. The sulfur compound was used on the structural prisms to ensure that the grout was fully engaged in carrying the load. The perlite grout was not considered to add to the strength of the prisms; therefore, fiberboard caps were sufficient to transfer the load to the blocks.

Compressive Strength

Three prisms from both grouting methods were tested in compression, in substantial accordance with ASTM C1314 (ASTM International , 2013), over one year. The resultant average compressive strengths for the two grouting methods are shown in Figure 12. In this figure, the compressive strength is taken as the ultimate load divided by the gross cross-sectional area of the block, which was approximately 119 in^2. For reference the standard design value for a portland cement CMU is 1500 psi. In the structural- and perlite-grouted specimens, the failure mechanisms of the blocks were similar and initiated with a failure in the mortar joint and progressed through the block shell (Figure 13), and culminated with the CMU shell falling off and the grouted core remaining (Figure 14).

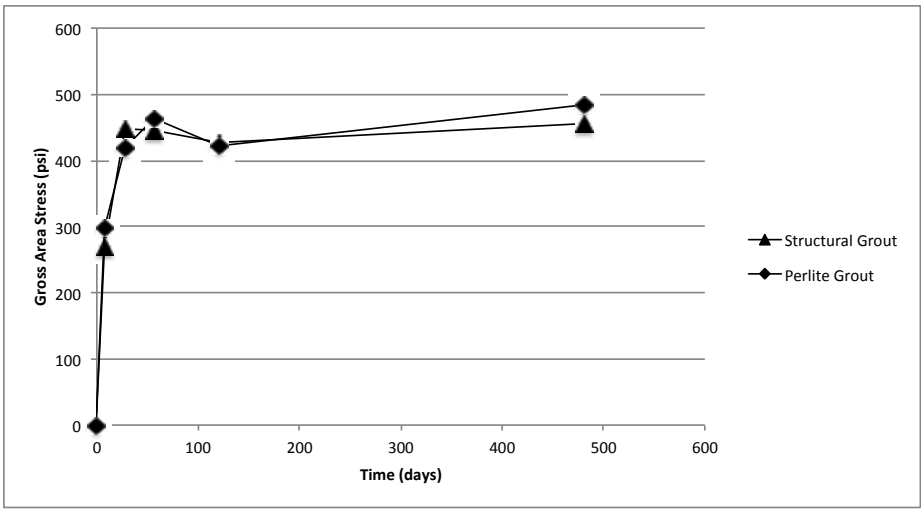

Figure 12. Prism compressive strength vs prism age

Figure 13. Typical prism failure

(a) (b)

Figure 14. Ultimate failure of (a) perlite prism and (b) structural prism

Referring to Figure 12, the structural- and the perlite-grouted prisms had similar overall compressive overall strengths on each day. This result is somewhat unexpected, as the perlite grout was not anticipated to carry any of the load; therefore, the perlite grouted specimens were expected to have a smaller effective cross-sectional area, and thus have smaller ultimate loads and smaller strengths (the strengths are the ultimate loads divided by the gross areas). It should be noted, that if the effective areas are used to calculate the stress rather than the gross areas, as is done in the following chapters, the compressive stresses of the perlite-grouted prisms would exceed those grouted with structural grout. The similar strengths between grouted prisms may be partially due several different factors. Shrinkage between the structural grout and the cell walls could lead to a loss in load transfer and therefore a lower capacity. Further, the structural grout may have a significantly lower stiffness relative to the block, and thus may not be contributing much to the strength of the prism. It is also worth noting that these prisms

failed at axial loads similar to the axial loads observed for the standard blocks discussed in the previous chapter (approximately 55 to 60 kips). The discussion above indicates that both the structural grout and the perlite grout have little to no effect on the compressive strengths of the prisms, and therefore it may not be appropriate to include the area of the grout in stress calculations.

Modulus of Elasticity

The modulus of elasticity of the prisms was determined in substantial accordance to ASTM E111 (ASTM International, 2013) by loading the specimens to 33 percent of their expected capacities while recording the applied load and the resultant deflection of the prism, as observed in Figure 15. The deflection was monitored with two potentiometers attached to the top and bottom of the prisms using epoxied brackets.

Figure 15. Modulus of elasticity test setup

The average measured modulus for the prisms made with each type of grout is shown in Figure 16. For reference, included in this figure are the predicted moduli based on the compressive strength of the prism (Schneider & Dickey, 1994). In particular the predicted moduli were calculated as $E_m = 900f'_m$, where f'_m is masonry compressive strength in psi. As can be seen in Figure 16, after an initial gain, the structural- and perlite-grouted prisms maintained a relatively constant moduli throughout the test series. The perlite-grouted blocks were observed to be slightly stiffer than the perlite-grouted specimens, with an average moduli of around 358,500 psi, while the structural-grouted specimens had an average moduli on each day of around 314,300 psi. In regards to the effectiveness of the predicted modulus equation, both the structural- and perlite-grouted specimens had moduli less than the code predicted approximation on all days. At the culmination of testing, the predicted moduli were 23% and 18% higher for the structural and perlite specimens, respectively. This indicates that this material is less stiff than conventional portland cement based block with similar compressive strengths.

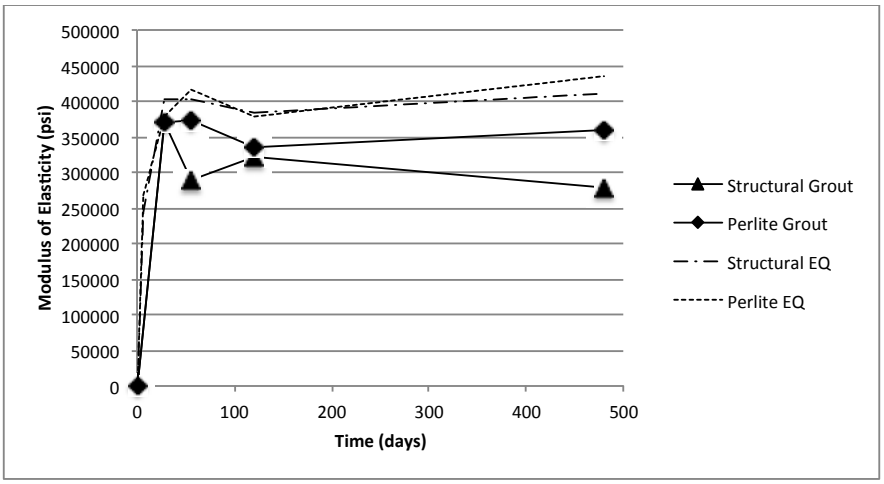

Figure 16. Prism modulus of elasticity vs prism age

Tensile Testing

It is difficult to directly measure the tensile capacity of masonry assemblies; therefore, the tensile capacities were inferred through unreinforced bending tests. In this research, two masonry layups were tested for each grouting method. These layups consisted of a simple 4-block prism (Figure 17), and a double-wythe 6-course running-bond assembly (Figure 18). The nominal dimensions of the 4-block prisms were 16-by-8-by-32 inches, while the nominal dimensions of the 6-course assemblies were 24-by-16-by-48 inches. These assemblies were constructed by experienced masons on the same day as the wall assemblies discussed in the following chapter, and were cured alongside the wall specimens at room temperature in dry conditions.

Figure 17. 4-block prism prior to grouting

Figure 18. 6-course running bond layup prior to grouting

These layups were tested lengthwise in three-point bending about their strong axes until failure, while monitoring the applied load (Figure 19). The tensile stress (f_t) is then calculated from the maximum-recorded load by determining the moment at failure (*M)* and then calculating the tensile stress in the extreme bottom fiber at this moment, assuming a linear-elastic material response. That is, the tensile stress is calculated as $f_t = \frac{M}{S}$, where *S* is the section modulus of the assembly. In these calculations, the self-weight of the specimens is considered, and the section moduli were obtained from values published by the National Concrete Masonry Association (2003). Specifically, the section moduli for the perlite-grouted specimens are based on ungrouted values, while the structural specimens values are assuming that the specimens are fully grouted. Also, it

should be noted that the NCMA method assumes that the stiffness of the block matches that of the grouts (i.e., the method of transformed sections is not used).

Figure 19. Tensile specimen prior to testing

A total of three specimens per layup were tested for each grouting method around the same time the wall specimens were tested, which corresponded to 480 days after casting. The average tensile stresses of these specimens is provided in Table 2. Included in this table are the predicted stresses based on the measured compressive strengths of the 2-block prisms (from a previous section). In particular, this stress is calculated as $4 \times \sqrt{f'_m}$ (Schneider & Dickey, 1994).

Table 2. Tensile capacity of masonry systems

Beam Layup	Tensile Stress (psi)	
	Structural Grout	Perlite Grout
4-Block Prism	110	31
6-Course	179	77
Expected	85	88

For both grouting methods, the 6-course assemblies had significantly higher tensile stresses than the 4-block prisms, with values 69% and 150% higher for the structural grout and perlite grout, respectively. This is somewhat unexpected, as the differences in geometry should have been accounted for by the section moduli.

In regards to the effect of the grouting method, the structural-grouted specimens had a higher tensile capacity than the perlite-grouted specimens for both layups. In particular, the structural-grouted specimens were 3.5 and 2.3 times stronger than the 4-block and 6-course perlite-grouted specimens, respectively. This too is somewhat unexpected, as the lack of structural grout should have been accounted for by the reduced section moduli of the perlite-grouted specimens. Further, the grouting method had no noticeable effect on the prism compressive strength in the previous section.

Regarding the efficacy of the predicted tensile strength equation, both of the structural-grouted layups had tensile strengths that exceeded the predicted values. The 4-block prism strengths were 35% higher than predicted, while the 6-course layup strengths were 110% higher. Both of the perlite-grouted specimens were less than expected based on their compressive strength.

The trends above were also observed in the structural wall tests. Potential reasons for these trends are discussed in greater detail in the following chapter.

STRUCTURAL TESTING

A total of five wall specimens were constructed and tested in this research to determine the in-plane shear resistance of lime CMU walls, and to determine the applicability of existing design codes in this respect. In this chapter, the testing method is presented first, followed by a description of the test setup and instrumentation. Test results for each wall are then presented and discussed.

Testing Matrix

A total of five 4-foot tall by 4-foot long walls were tested, which consisted of two single-wythe walls and three triple-wythe walls. Note that while walls with a smaller height-to-length aspect ratio may have been more desirable for in-plane shear testing without axial load, the dimensions of the walls were constrained by thermal resistivity testing requirements. That is, as mentioned in the introduction, another objective of the overall project was to determine the thermal resistivity of the lime CMU walls; this restricted the dimensions and weight of the walls to those that could fit and be transported to the thermal lab. A summary of the wall specimens tested in this research is provided in Table 3.

Table 3. Wall specimen testing matrix

Wall Specimen	Grouting Method	# of Wythes
SP	Perlite	1
SS	Structural	1
TP	Perlite	3
TPS	Perlite/Structural	3
TS	Structural	3

The two single-wythe wall specimens consisted of one grouted with perlite grout (SP) and one grouted with structural grout (SS). The three triple-wythe wall specimens consisted of one grouted solely with perlite grout (TP), one grouted with half perlite and half structural grout (TPS), and one grouted solely with structural grout (TS). These wall sections were selected to bracket the behavior of the possible wall configurations that were to be used in construction. Each wall specimen was fully grouted and unreinforced, and was constructed using a running bond orientation. The decision to make these walls without reinforcement was made by the owner in conjunction with Virginia Lime Works. One of the primary objectives of using hydraulic lime was the desire to create an extremely durable and all-natural masonry system that would be breathable and allow for moisture transport through the wall (no vapor barrier); therefore, concerns were raised regarding rebar corrosion.

The block layups for the various wall specimens are shown in Figure 21 and Figure 22, and the grouting pattern for the wall consisting of perlite and structural grout (TPS) is shown in Figure 23. The walls were constructed on top of steel base plates that were designed to be post-tensioned to the floor (Figure 20). These plates had shear tabs that were located such that they would line up with the cells of the CMU walls, as indicated in Figure 21 and Figure 22. A conventional portland cement grout was used in the bottom half of the base course of the wall around these shear tabs. This was done to ensure that the failure mechanism would be forced into the main wall and not simply reflect a poor connection between the wall and the base.

Figure 20. Wall assembly base

The wall specimens were constructed by experienced masons using the standard lime CMU blocks discussed in a previous chapter, and the Wisconsin lime was used as the binder in the mortar and grout. The walls under various stages of construction are shown in Figure 24. Upon assembly, the walls were then cured at room temperature under dry conditions in the structures lab until the day of testing, which was at 400 days after casting. Note that in the interim some of these wall panels were subjected to thermal testing.

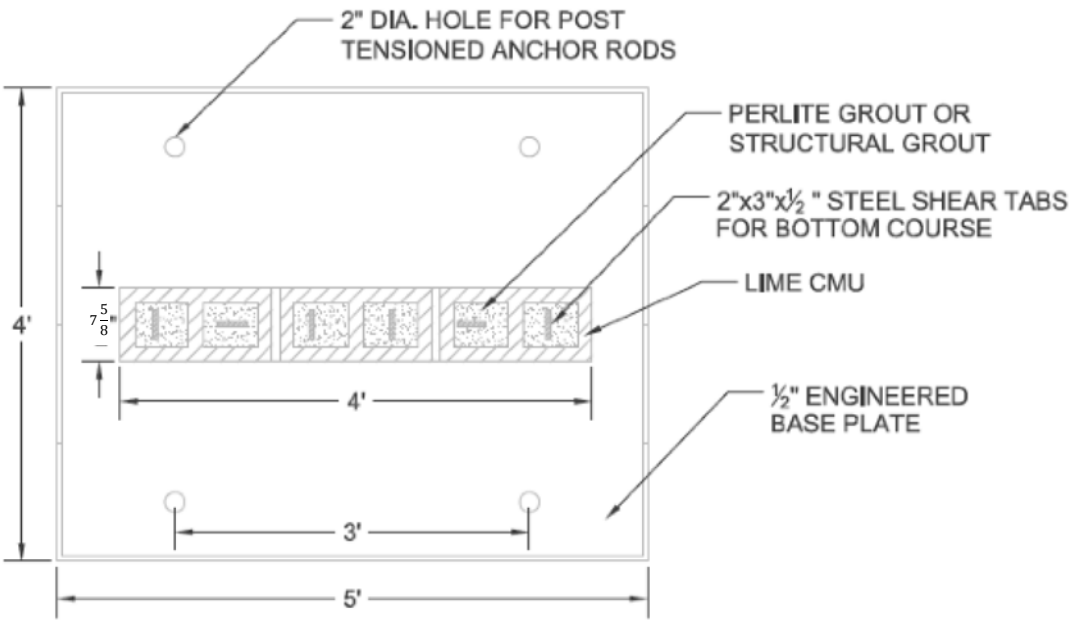

Figure 21. Typical wall specimen and grouting pattern for single-wythe walls

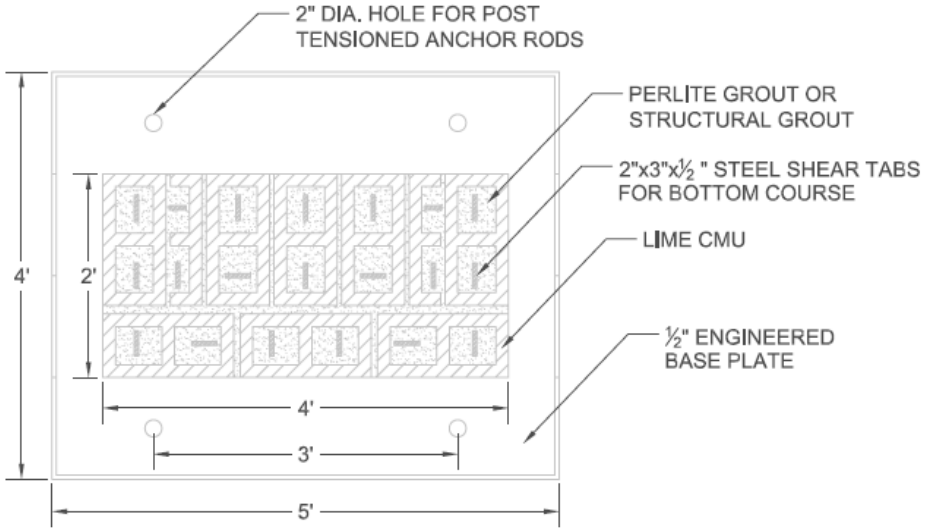

Figure 22. Typical wall specimen and grouting pattern for triple-wythe walls

Figure 23. TPS wall after grouting

Figure 24. Wall specimens under construction

Test Setup

Each wall specimen was tested in substantial accordance to ASTM C1717-12 (ASTM International, 2013) for in-plane masonry shear strength. Each wall specimen was loaded in plane with a pseudo-statically applied lateral load until failure, while monitoring the applied load and resultant deflections. The load frame used in this testing is shown in Figure 25, while the actual load setup is shown in Figure 26. It should be noted that no axial load was used in this test setup in part because the CMU walls in the proposed construction project were designed to carry only shear, and no axial load beyond their self weight.

As can be observed in this figure, a reinforced concrete cap was constructed on top of each wall specimen using a 5,000 psi portland cement concrete mix. The caps provided a location to apply the load without prematurely damaging the wall specimen. Dowels were placed in the top course of the wall and monolithically cast with the cap to provide load continuity between the cap and the wall. It should also be noted that the load frame and wall base plate were post-tensioned to the floor prior to testing.

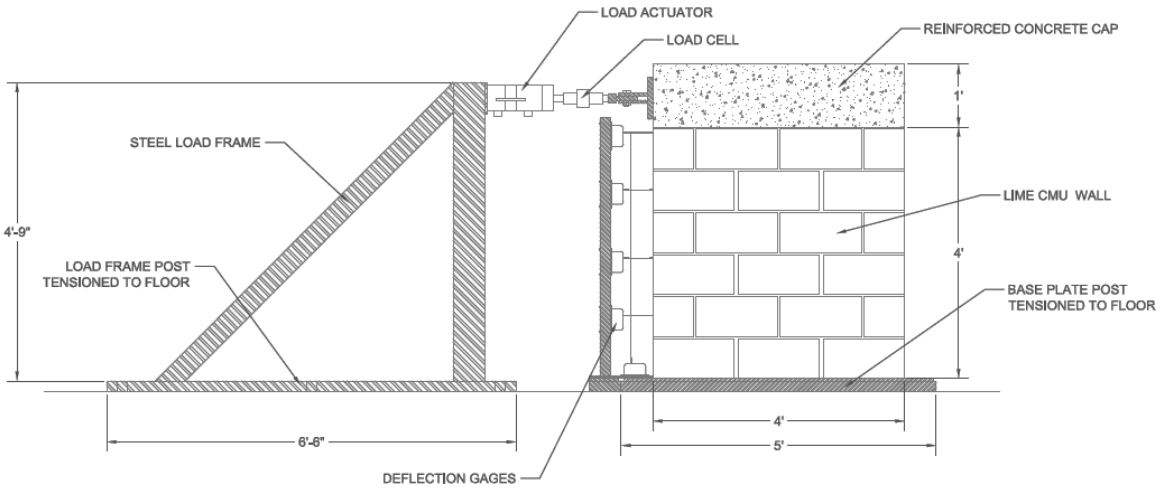

Figure 25. Test setup and instrumentation

Figure 26. Wall test setup prior to testing

Instrumentation

The load was monitored with a load cell mounted to the actuator, as indicated in Figure 25. The lateral deflection was monitored at quarter points up the height of the wall with four linear string potentiometers as shown in Figure 25, while a single potentiometer measured the vertical uplift of the wall at the point indicated.

In addition to monitoring the load and deflection, the strain fields in the wall were monitored continuously throughout the loading with an Aramis – 3D Deformation Measurement System. Generally speaking, this system works by monitoring the relative location of black dots painted on the side of the test specimens, and then post processing this data to determine normal and shear strains. This data was particularly helpful in determining the failure mechanism of each wall, tracking crack propagation, and viewing stress concentrations.

Test Results

The test results for the wall specimens are discussed in this section. First, the results of each individual wall are discussed separately, followed by a summary of the key findings.

Single Perlite – SP

The single-wythe wall with perlite grout was tested first in this research, and was expected to be the weakest of the five walls. The wall specimen at commencement of the test is shown in Figure 27a, while the wall immediately after failure is shown in Figure 27b. The applied load versus the deflection of the top of the wall is shown in Figure 28.

This wall failed at a load of approximately 2.0 kips due to the formation of a horizontal crack in the mortar line near the top of the wall that then propagated across the wall until it reached the compression zone on the far side of the wall, at which point the crack propagated diagonally downward (Figure 27b). The peak top displacement at ultimate load was 0.034 inches, and the peak uplift displacement was 0.02 inches.

In terms of the force-deflection behavior, the wall behaved linear until failure due to the formation of the crack discussed above. The applied lateral load then decreased slightly and then remained constant as the deflection increased. This type of post-failure response typically indicates a ductile failure; however, this was not the case in this test. Upon failure, the top portion of the wall began to slip relative to the base. The resistance after failure is due in part to the friction across this crack, and in part due to the slight uplift forces. The fact that the friction force is only slightly less than the force required to shear this top portion of the wall off indicates that the mortar has very little shear capacity. However, this crack may have initially commenced do to the combination of the tensile forces due to uplift and the shear stresses.

(a) (b)

Figure 27. SP wall: (a) before loading and (b) after loading

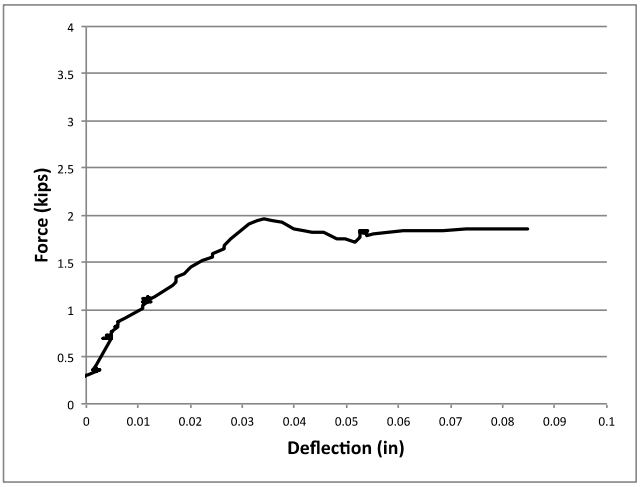

Figure 28. Force-deflection response of SP wall

Figure 29a-d shows the observed normal-strain field (in the vertical direction, ε_y) at various stages of loading. As can be observed in this figure, the initial crack that caused failure became evident in this strain data at around 1.8 kips, slightly before the ultimate failure. The presence of these normal-strain concentrations prior to failure

indicate that these cracks may have initiated due to the slight uplift force prior to shearing.

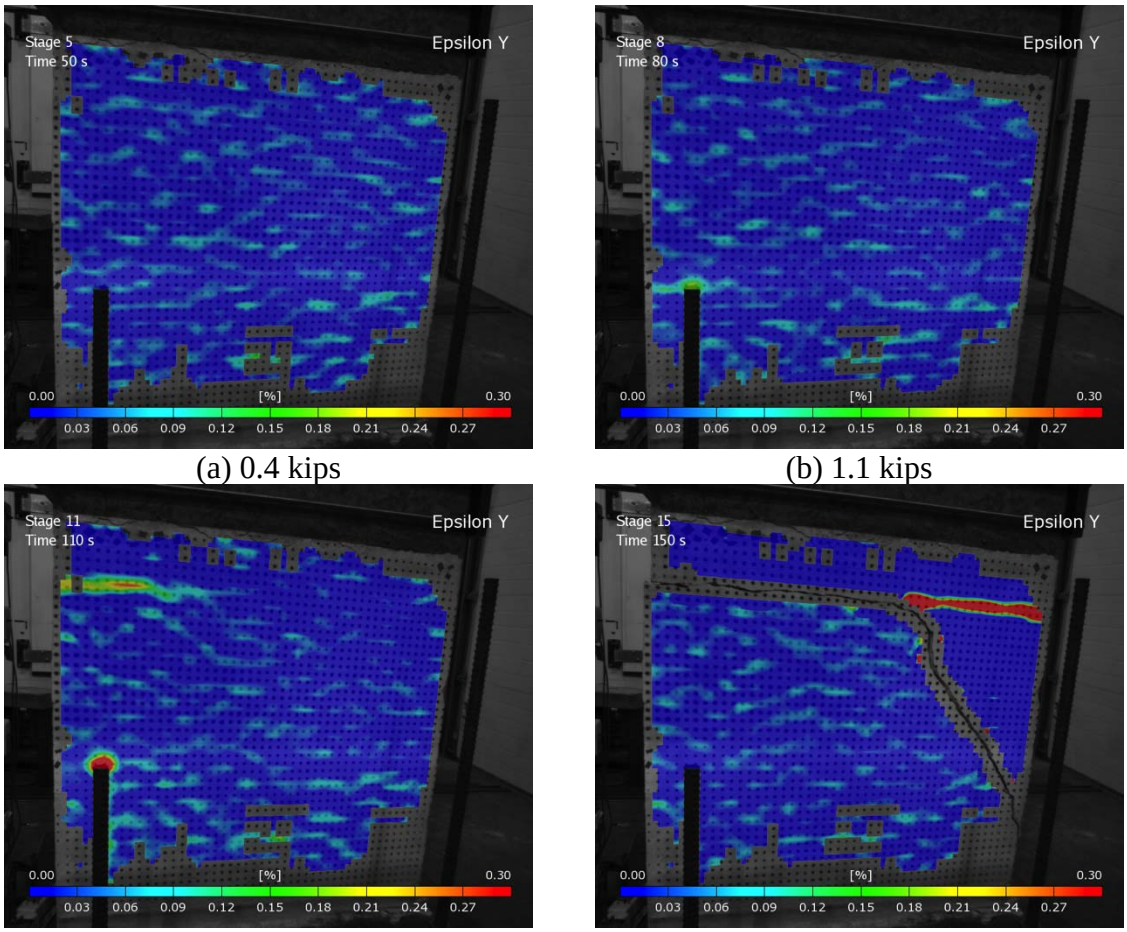

(a) 0.4 kips (b) 1.1 kips

(c) 1.8 kips (d) 0.9 kips

Figure 29. Vertical normal-strain fields (ε_y) observed in the SP wall at various load stages

Single Structural – SS

The second wall that was tested was the single-wythe wall with structural grout – SS. Figure 30 shows the condition of the wall at failure, while the force-top deflection

response of the wall is provided in Figure 31. This wall failed in a similar fashion as the SP wall; that is, it failed due to the formation of a horizontal crack on the mortar line near the top of the wall (Figure 30) at a lateral of around 3.5 kips. In regards to the force-deflection behavior, the wall behaved linearly until failure, at which point the lateral load decreased to a value around 2.0 kips. This load is approximately the same load that the SP wall sustained after the initial crack formed. Indicating that the friction force was similar for both the SP and SS walls after the formation of the initial crack. The lateral and uplift displacement at failure were observed to be 0.015 and 0.005, respectively.

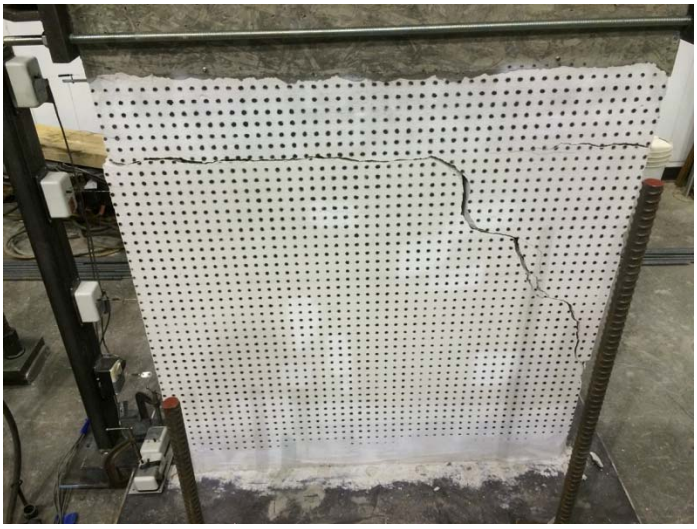

Figure 30. SS wall after failure

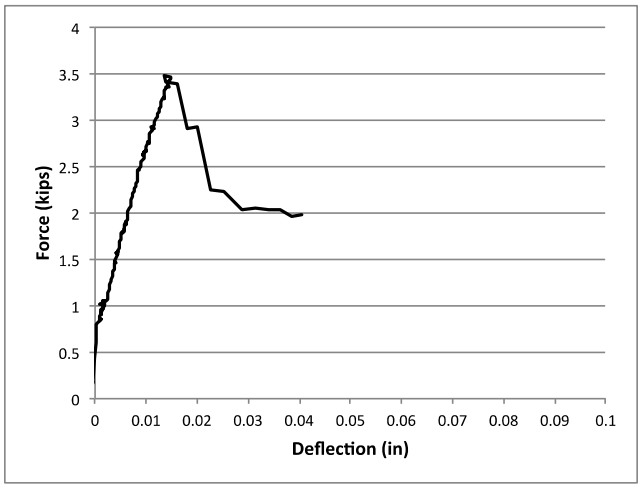

Figure 31. Force-deflection response of SS wall

The normal-strain fields (in the vertical direction, ε_y) in the wall at various load stages are shown in Figure 32. As was the case with the SP wall, the horizontal crack is evident in these images prior to cracks becoming visible and prior to the ultimate load. Further, the existence of these normal strains indicates that the tensile strains from uplift may have initiated the crack prior to it propagating in shear.

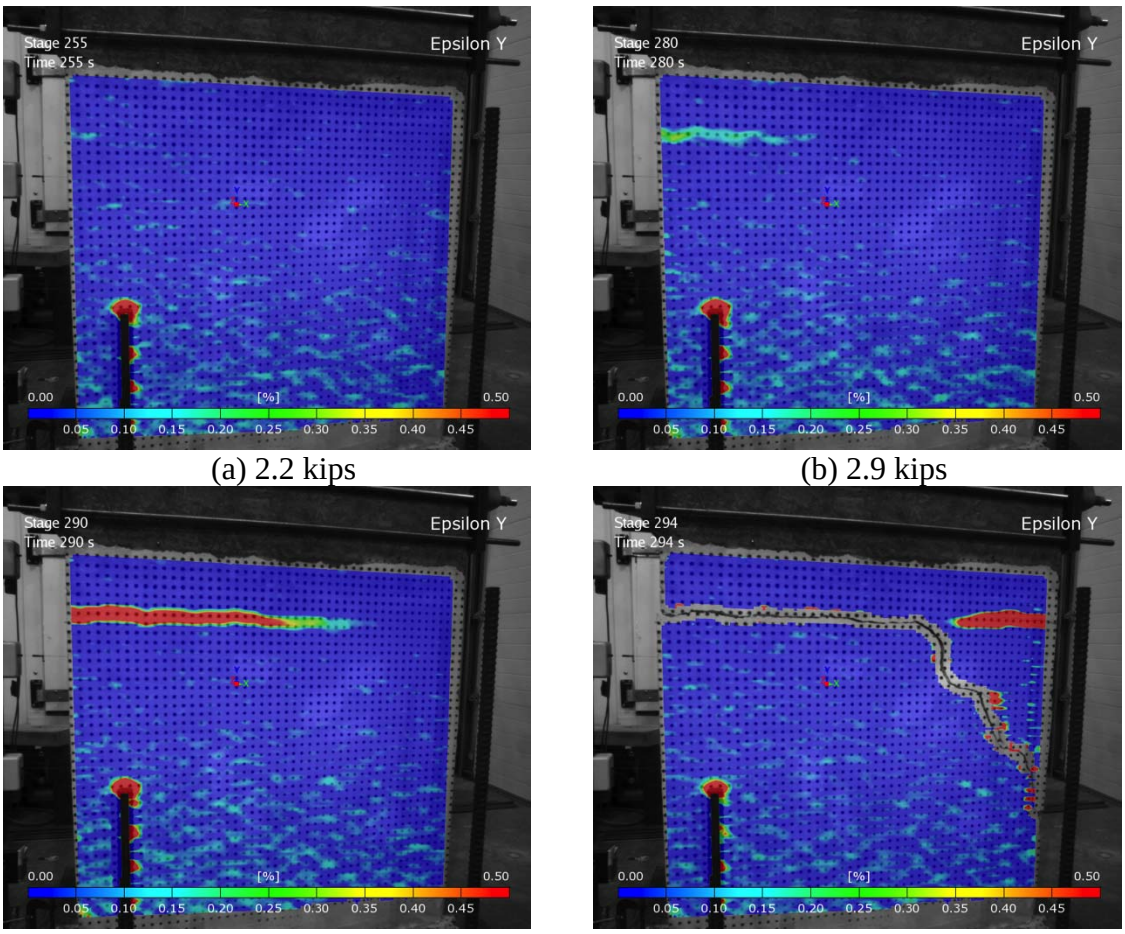

(a) 2.2 kips (b) 2.9 kips

(c) 3.1 kips (d) 3.2 kips just after failure

Figure 32. Vertical normal-strain fields (ε_y) observed in the SS wall at various load stages

Triple Perlite – TP

The third wall that was tested was the triple-wythe perlite grouted wall – TP. The wall immediately after failure is shown in Figure 33, and the force-deflection response of the top of the wall is shown in Figure 34. This wall failed at a load of approximately 2.5 kips due to the formation of a horizontal crack near the base of the wall on a mortar line. This crack initiated on the side of the wall closest to the lateral load, and then propagated

across the wall. It should be noted that in the process of transferring the TP wall between the thermal testing lab and the structures lab, some damage was sustained in the form of a small crack in the mortar joint at this same location. Indicating that this crack may have initiated prior to testing. Similar to what was observed in the single-wythe walls, the top portion of the wall then began sliding relative to the base after reaching the peak load. The maximum lateral and uplift displacements at failure were 0.028 inches and 0.022 inches, respectively.

In regards to the force-deflection response, the wall behaved linearly until the formation of the crack at the base. Again, although this force-deflection response typically indicates a ductile failure mechanism, this is not the case for this wall. As was mentioned previously, the wall began slipping and this force after failure is most likely due to the friction between these two wall sections.

The strain fields (in the vertical direction, ε_y) within the wall at multiple load levels are shown in Figure 35. As was the case in the single-wythe walls, a normal-strain concentration can be observed at the base of the wall prior to the crack becoming evident at this location. This strain concentration indicates that this crack initiated due to uplift.

Figure 33. TP wall after failure

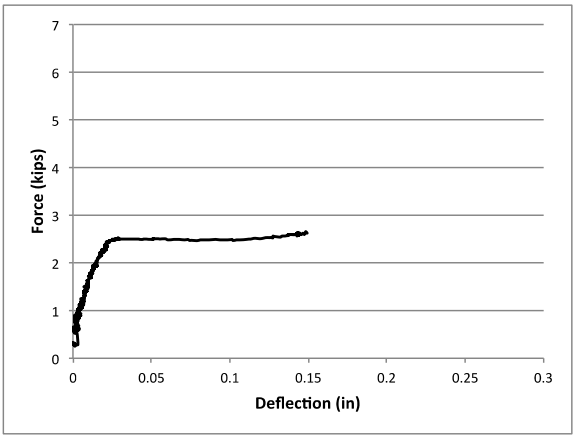

Figure 34. Force-deflection response of TP wall

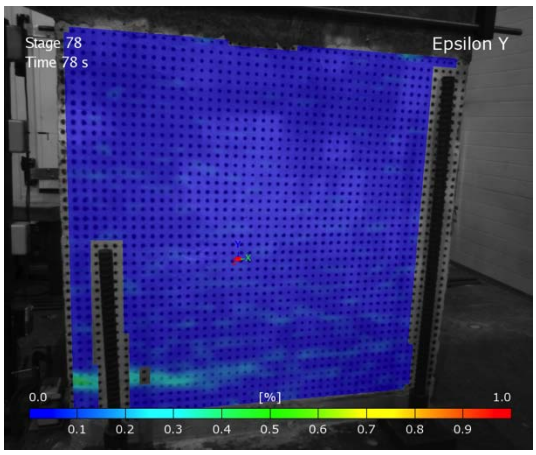

(a) 0.9 kips

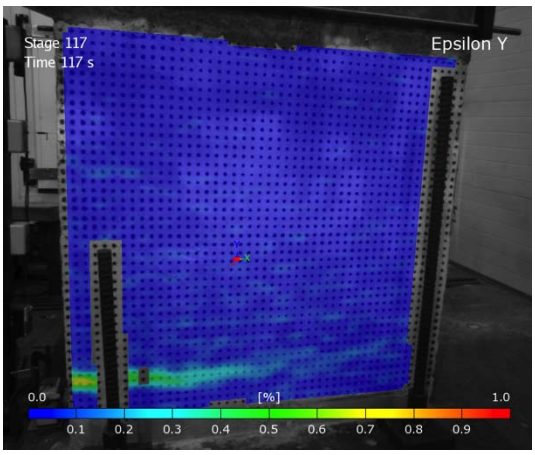

(b) 1.4 kips

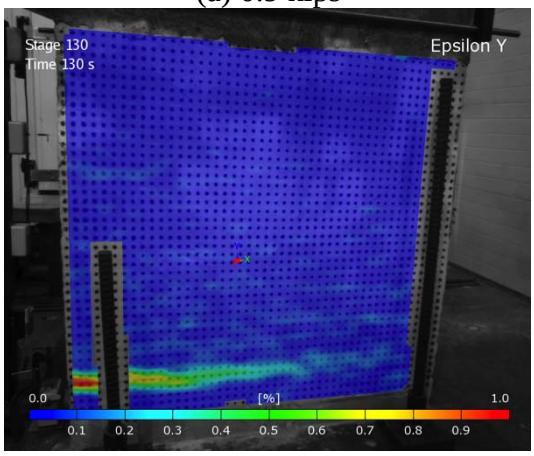

(c) 1.9 kips

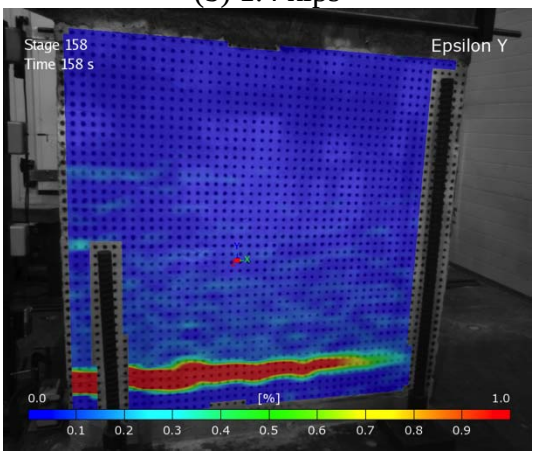

(d) 2.5 kips just prior to failure

Figure 35. Vertical normal-strain fields (ε_y) observed in the TP wall at various load stages

Triple Perlite/Structural – TPS

The fourth wall that was tested was the triple-wythe wall with a mix of perlite and structural grout – TPS. Figure 36 shows the condition of the wall at failure, while the force-versus-tip deflection response of the wall is provided in Figure 37. This wall failed in a similar fashion as the TP wall near the base of the wall at a load of approximately 4

kips. The lateral deflection and uplift deflection at failure were approximately 0.033 and 0.026 inches, respectively.

The force-deflection response of the wall was linear until the formation of the crack, at which time the applied load decreased to approximately 3.0 kips and then sustained this load. Again, this sustained 3-kip load is most likely the friction force caused by the wall slipping.

Figure 36. Failure surface of TPS wall

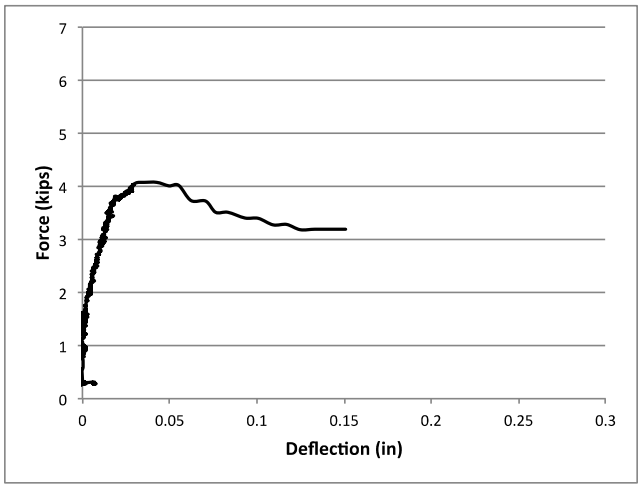

Figure 37. Force-deflection response of TPS wall

As was done for the previous walls, the normal-strain fields (in the vertical direction, ε_y) at various load stages are shown in Figure 38. Again, strain concentrations can be observed in this data, prior to this crack becoming visible. This concentration is observable at the base of the wall as early as 1 kip. These strain fields show the failure mechanism to be a tensile crack formed by uplift.

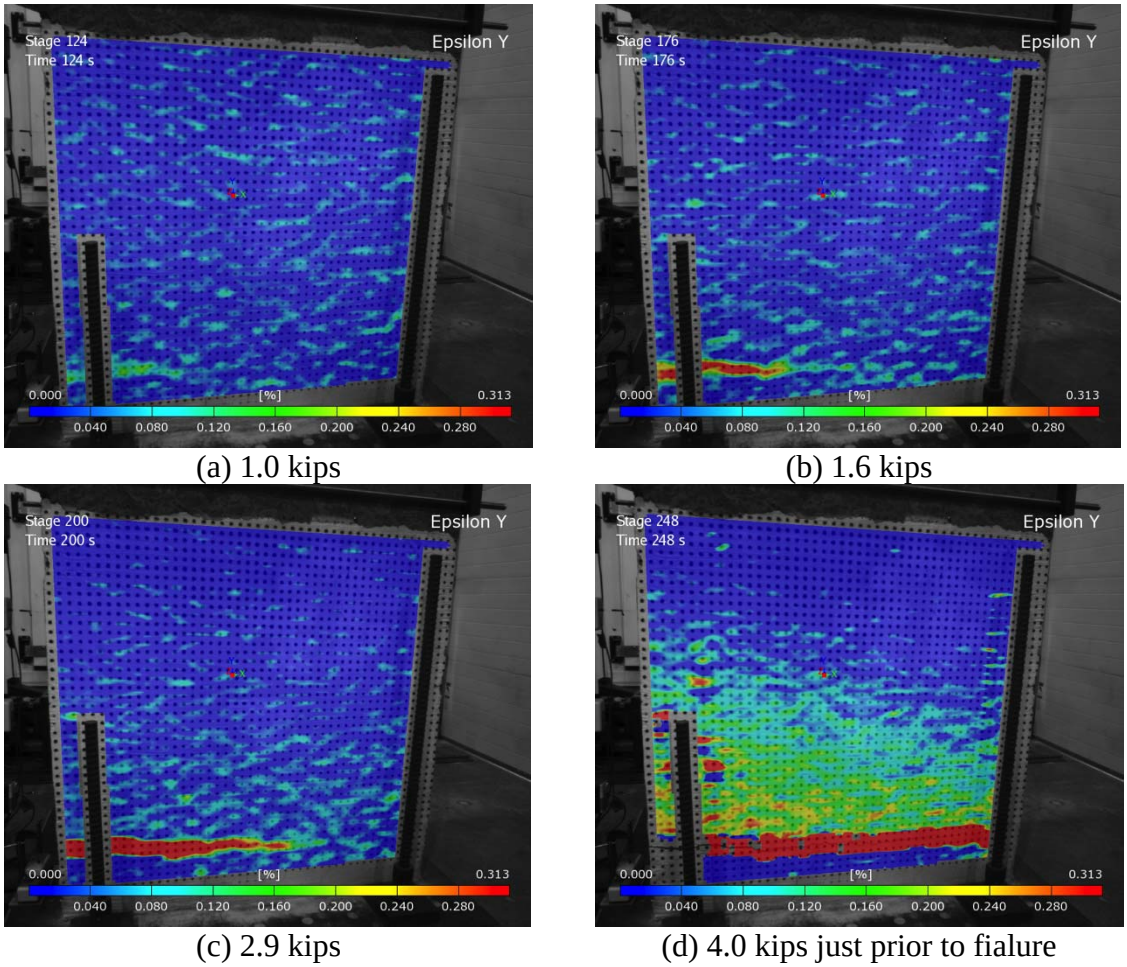

(a) 1.0 kips (b) 1.6 kips

(c) 2.9 kips (d) 4.0 kips just prior to fialure

Figure 38. Vertical normal-strain fields (ε_y) observed in the TPS wall at various load stages

Triple Structural – TS

The last wall to be tested was the triple-wythe wall with structural grout – TS. The condition of the wall after failure is shown in Figure 39, and the force-versus-tip deflection is provided in Figure 40. This wall failed in a similar fashion as the TP and TPS walls, with a crack initiating in the mortar joint between the second and third course on the side of the applied load that then propagated across the wall. It failed at a load of

approximately 6.7 kips. The lateral deflection and uplift deflection at failure were approximately 0.067 inches and 0.010 inches, respectively.

The force-deflection response is linear until the point of first crack, at which time the wall's load carrying capacity decreased substantially. It should be noted, that the brittle nature of this failure caused some data acquisition issues. That is, some of the data points immediately after failure were erroneous and were culled from the data. The capacity of the wall system decreased until it reached approximately 4 kips, and then sustained this load until the test was terminated. As with the other walls this sustained force is likely due to the friction between the two wall sections.

Figure 39. TS wall after failure

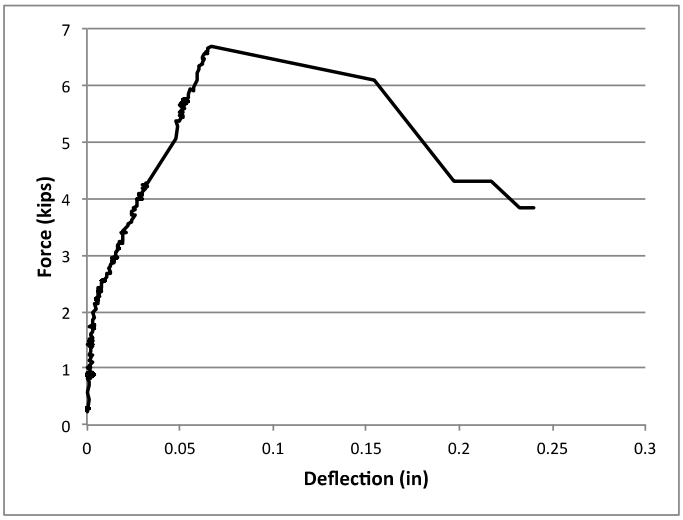

Figure 40. Force-deflection of TS wall

As was done for previous walls, the normal-strain fields (in the vertical direction, ε_y) for various load stages are shown in Figure 41. Stress concentrations become visible on the strain field before the cracks were visible on the wall. These strain concentrations first become visible as early as 2.3 kips. These normal-strain concentrations indicate a tensile failure due to uplift.

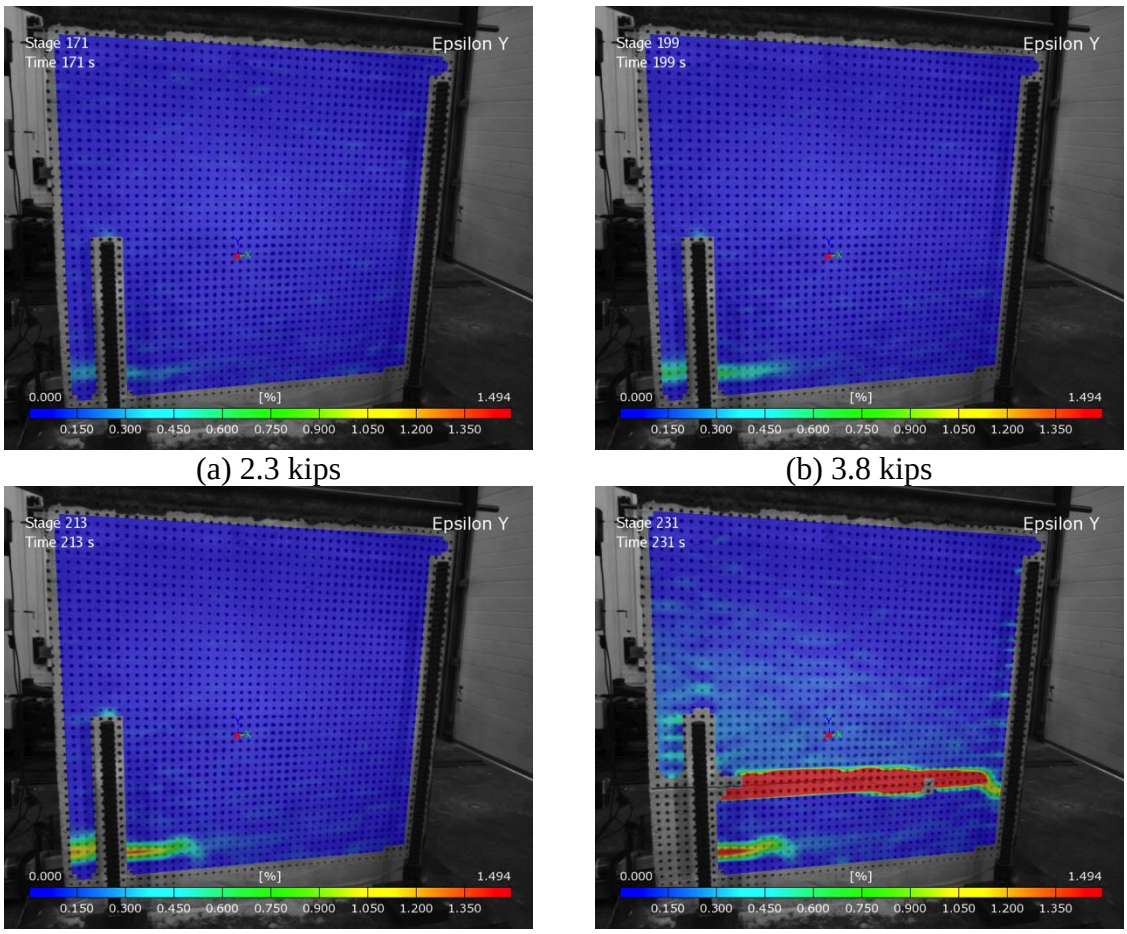

(a) 2.3 kips (b) 3.8 kips

(c) 5.7 kips (d) 6.7 kips just prior to failure

Figure 41. Vertical normal-strain fields (ε_y) observed in the TS wall at various load stages

Discussion of Results

The results from the in-plane shear tests for each wall specimen are summarized in Table 4, while the force-deflection responses for the single-wythe and triple-wythe walls are provided in Figure 42 and Figure 43.

Table 4. Summary of in plane wall testing

Wall Specimen	Moment Arm (in)	Max Load (kips)	$\Delta_{tip\ max}$ (in)	$\Delta_{uplift\ max}$ (in)	A (in^2)	S (in^3)	$\sigma_{tension,\ failure}$ (psi)	$\sigma_{tension,\ perdicted}$ (psi)
SP	13.5	1.95	0.034	0.020	120	324	77	88
SS	13.5	3.19	0.015	0.005	366	465	100	85
TP	45.5	2.52	0.028	0.022	360	972	111	88
TPS	45.5	4.08	0.033	0.026	744	1192	152	na
TS	37.5	6.69	0.067	0.010	1098	1396	178	85

All walls in this test series failed do to the formation of a horizontal crack due to uplift forces, which then propagated across the wall until the top portion of the wall sheared from the base. As can be observed in Figure 42 and Figure 43, this type of failure resulted in a linear-elastic force-deflection response until failure, and then after some loss in load the walls would sustain a constant force with increasing deflections. This sustained load after failure is most likely due to friction forces exerted while the top portion of the wall was sliding along the horizontal crack interface.

In terms of the relative total lateral-load capacity, the walls behaved as expected. That is, the structural-grouted walls had capacities greater than their perlite-grouted counterparts, and the wall grouted with a mixture of perlite and structural grout had a capacity that was bracketed by the structural- and perlite-grouted walls. Further, the structural-grouted walls had higher initial stiffnesses than the walls grouted with perlite or the walls grouted with a mixture of perlite and structural grout.

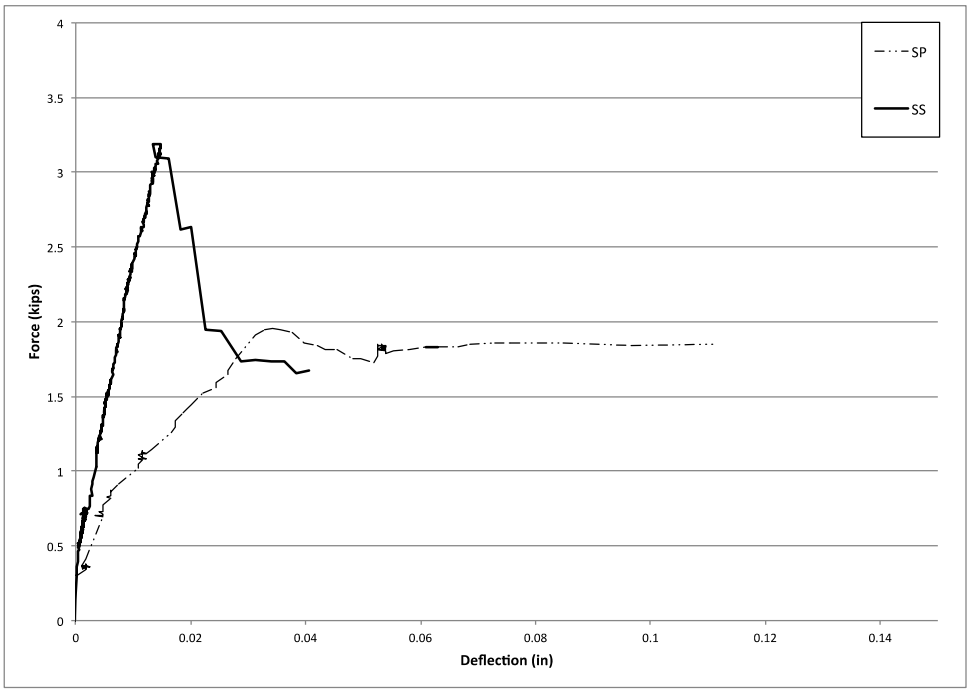

Figure 42. Force-deflection response of single-wythe walls

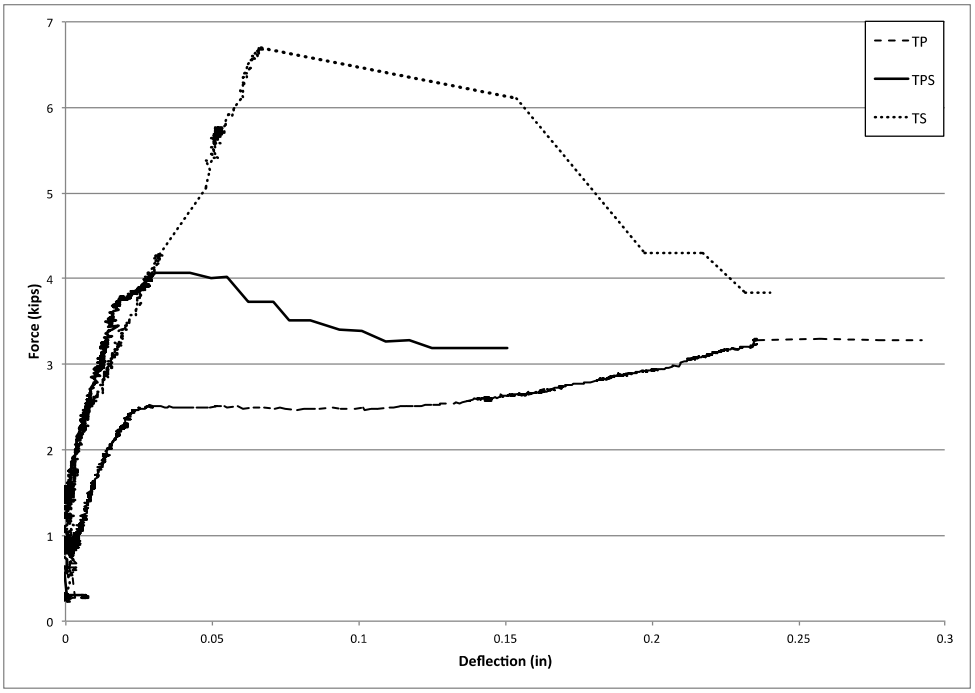

Figure 43. Force-deflection response of triple-wythe walls

An attempt was made to calculate the tensile stresses observed in the walls at the formation of the initial horizontal crack, and then to compare these stresses to those obtained in the tensile tests discussed in the previous section, as well as predicted values based on compressive strength. Included in Table 4 are the tensile stresses calculated at failure assuming a linear-elastic response prior to failure. In particular, these stresses were calculated based on simple mechanics with the following equation.

$$\sigma = \frac{P}{A} - \frac{M}{S}$$

where *P* is the axial load, *A* is the effective base area of the wall, and *S* is the effective section modulus of the wall. The effective areas and section moduli of the walls used in these calculations were obtained from values published by the National Concrete Masonry Association (2003) and are also included in this table. The effective areas and section moduli for the perlite-grouted specimens are based on ungrouted specimens, while the structural specimens values are assuming that the walls are fully grouted. The values used for the TPS wall assumes that the wall is grouted every-other cell, which is 16 inches on center.

As can be observed in this table, the structural-grouted walls obtained a higher apparent tensile stress than their perlite counterparts, and the TPS wall had a stress that was between the TS and TP walls. This trend is somewhat unexpected, as one might anticipate these stresses to be fairly close to each other because the effect of the grout should have been taken into consideration with the effective areas used in the stress calculations. This discrepancy indicates that the structural grout may provide additional benefits beyond assisting in carrying the applied loads. That is, the grout may be helping

to support the blocks, thus preventing premature failures. Further, this discrepancy may be due other stresses exerted on the blocks beyond what are considered with the above equation (i.e., shear) and the structural grout may be more effective at resisting this combination of these shear and normal stresses.

In comparing the single- and triple-wythe walls it can be observed that the triple-wythe walls have significantly higher tensile stresses than their single-wythe counterparts. This too is somewhat unexpected, as the differences in geometry between these specimens should be accounted for with the areas and section moduli. This result may indicate that there are added benefits to the additional wythes of block. Similar to what was discussed for the effect of grout, these additional blocks may act to stabilize the blocks and may be more effective at resisting both the shear and normal stresses exerted on the walls.

Both of these trends were also observed for the tensile test assemblies discussed in the previous chapter (Table 2). That is, the structural-grouted specimens had higher tensile stresses than the perlite specimens, and the double-wythe running-bond buildups had tensile stresses higher than the single-wythe prisms. It should also be noted that the tensile stresses for the structural-grouted walls were quite similar to the corresponding tensile stresses of the structural-grouted tensile specimens. That is, the SS wall had a stress of 100 psi while the 4-block prism had a capacity of 110 psi, and the TS wall had a capacity of 178 psi and the 6-course running bond layup had a capacity of 179 psi. This was not the case for the perlite-grouted specimens.

In regards to the efficacy of the predicted tensile stress equation based on compressive strength of prisms, $4 \times \sqrt{f'_m}$ (Schneider & Dickey, 1994), all specimens had observed tensile-stresses that exceeded their corresponding predicted stresses, with the exception of the the single-wythe perlite wall.

The discrepancies discussed above may also point to issues associated with the basic mechanics used in predicting these failures; for example, only normal stresses associated with axial load and moment were considered, and the effective areas and section moduli used in these calculations may not be appropriate for lime masonry components. That is, the effective areas and section moduli prescribed by the NCMA assume that the grout and block have similar stiffnesses, and therefore gross section properties are used rather than implementing the method of transformed sections. However, this may not be appropriate for lime masonry components, as their relative stiffnesses may not be similar.

SUMMARY AND CONCLUSIONS

With the ever-increasing emphasis on making construction a greener enterprise, it is important to investigate new construction practices that may lead to less carbon emissions and less energy consumption. One such practice may be using hydraulic lime as the sole binder in masonry systems in lieu of conventional portland cement. The production of hydraulic lime uses significantly less energy and emits fewer greenhouse gasses during its production than conventional portland cement. Further, hydraulic lime will actually absorb carbon throughout its lifetime.

In this thesis, the materials used in this research were evaluated first, followed by a characterization of the behavior of hydraulic lime CMU components (e.g., mortar and block) and assemblies (e.g., prisms). This research culminated with five in-plane shear wall tests. Based on this investigation, the following conclusions can be made.

1. One of the primary conclusions from this research is that it is possible to produce CMU blocks and components using hydraulic lime as the sole binder. In this research, a local block plant was able to produce hydraulic-lime CMU blocks with only slight modifications to their conventional mix designs and curing procedures.
2. The performance of hydraulic-lime CMU components is greatly affected by the lime source used as the binder. As was demonstrated in this research, the Ohio lime source performed significantly better than the Wisconsin lime. This is likely due to the higher quantities of calcium hydroxide and magnesium evident in the Ohio source, which have been known to contribute to hydration in the presence of

pozzolans. This hydration may explain the higher early strength gains observed in these blocks.

3. Better strengths were achieved in this research by dry curing specimens, rather than moist-curing them. This increased strength is most likely due to the fact that one of the primary strength-gain mechanisms in hydraulic lime is carbonization, and carbonization cannot occur at humidity levels higher than 75%. That being said, hydration is improved with moisture; therefore, some combination between the two curing methods may improve strengths further.
4. The effect of grout type on assembly performance was mixed. The compressive strength the prisms were nearly the same for both the structural- and perlite-grouted specimens. However, the structural-grouted specimens had higher capacities and resultant tensile stresses than the perlite-grouted specimens.
5. In the structural wall tests, the structural-grouted walls had higher ultimate loads than the perlite-grouted specimens, and the triple-wythe walls performed better than their single-wythe counterparts. These trends were also observed in the tensile stresses at failure, although this wasn't anticipated. This discrepancy is most likely due to the simplified mechanics used to calculate these stresses (i.e., the effect of shear is neglected).

This research demonstrated the feasibility of using hydraulic lime as the sole binder in CMU wall assemblies; however, further research is required to better characterize this material and improve its performance. Specifically, using the Ohio-sourced lime in the blocks, mortar, and grout may improve the component and structural

test results. Further alternate curing methods in which the specimens are cycled between moist- and dry-cure conditions may maximize strength by promoting both hydration and carbonization. Finally, expanded wall testing under more realistic conditions could provide better understanding of this system under lateral loads. Ideally, these tests would include walls with lower aspect ratios as well as axial loads. Additionally, it would be beneficial to investigate the performance of these walls with reinforcement, and if corrosion is a concern an alternate reinforcement (e.g., stainless steel, GFRP) may be considered.

REFERENCES CITED

ASTM International . (2013, August). C1072 Standard Test Measurement of Masonry Flexural Bond Strength. West Conshohoken, PA, USA.

ASTM International . (2013, August). C1314 Standard Test Method for Compressive Strength of Masonry Prisms. West Conshohocken, PA, USA.

ASTM International . (2013, November). C144 Standard Specification for Aggregate for Masonry Mortar . West Conshohcken, PA, USA.

ASTM International. (2013). C1019 Standard Test Method for Sampling and Testing Grout. West Conshohocken, PA.

ASTM International. (2013, August). C109 Standard Test Method for Compressive Strength of Hydraulic Cement Mortars (Using 2-in Cube Specimens). West Conshohocken, PA, USA.

ASTM International. (2013, June). C140 Standard Testing MEthods for Sampling and Testing Concrete Masonry Units and Related Units. West Conshohocken , PA.

ASTM International. (2013, October). C1552 Practice for Capping Concrete Masonry Units, Related Units and Masonry Prisms for Compression Testing. West Conshohocken, PA, USA.

ASTM International. (2013). C1713 Standard Specification for Mortars for the Repair of Historic Masonry. West Conshohcken , PA.

ASTM International. (2013, June). C1717-12 Standard Test Methods for Conducting Strength Tests of Masonry Wall Panels. West Conshohocken, PA, USA.

ASTM International. (2013, August). C33 Standard Specification for Concrete Aggregates . West Conshohocken, PA, USA.

ASTM International. (2013, December). C404 Standard Specification for Aggregates for Masonry Grout. West Conshohocken , PA, USA.

ASTM International. (2013). C90 Standard Specification for Loadbearning Concrete Masonry. West Conshohocken, PA.

ASTM International. (2013, August). E111 Standard Test Method for Young's Modulus, Tangent Modulus, and Chord Modulus. West Conshochocken, PA.

Ballard, J. R. (2012, April). Analysis of Unbonded Capping Material in Determining the Compressive Strength of Concrete Masonry Prisms. Brigham Young University .

Berry, M., Kappes, B., & Schroeder, D. (2014, May). REclaimed Asphalt Pavement as Aggregate in Portland Cement Concrete. *ACI Special Publication: Recycled Materials in Concrete, 2015, under review* .

Berry, M., Stephens, J., & Cross, D. (2011). Performance of 100% Fly Ash Concrete with Recycled Class Aggregate. *ACI Materials Journal* .

Cross, D., Stephens, J., & Berry, M. (2010). Sustainable Construction contributions from the Treasure State. *Concrete International , 32* (5), 41-46.

Graymont Western Lime Inc. (2013, September 13). Dolomitic Hydrated Lime, Type SA, Eden Plant. Eden, WI.

Greaymont Dollme Inc. (2012, May 29). Kemidol Dolomitic Hydrated Lime, Type SA, Genoa Plant. Genoa, OH.

Hartshorn, H. (2012). Dolomitic Lime Mortars: Carbonization Complications and Suseptibility to Acidic Sulfates . New York, NY: Columbia University .

Mertens, G., Snellings, R., Van Balen, K., Bicer-Simsir, B., Verlooy, P., & Elsen, J. (2008). Pozzolanic reactions of common natural zeolites with lime and parameters affecting their reactivity. *Elsevier Cement and Concrete Research* .

National Concrete Masonry Association. (2004). Compressive Strength Testing Variables For Concrete Masonry Units. 1. Herndon, VA.

National Concrete Masonry Association. (2007). Section Properties of Concrete Masonry Walls TEK 14-1B.

National Concrete Masonry Association. (2003). TEK 14-1A: Section Properties of Concrete Masonry Walls.

Oss, H. G. (2014). *Mineral Commodity Summaries - Cement.* U.S. Geological Survey. USGS.

Preuss, P. (2013, June 4). Roman Seawater Concrete Holds the Secret to Cutting Carbon Emissions. *Berkley Lab News Center* , 1-3.

Revie, W. (2013). Hydraulic Lime Binders - History and Comparison .

Schneider, R., & Dickey, W. (1994). *Reinforced Masonry Design.* Englewood Cliffs, NJ: Prentice-Hall, Inc.

Schork, J. (2012, November). Dolomitic Lime in the US History, Development and Physical Characteristics. *Journal of Architectural Conservation* .